ACCELERATING SPARSE CONVOLUTIONS IN VOXEL-BASED POINT CLOUD NETWORKS

Dionysios Adamopoulos 12

Anastasia Poulopoulou²

Georgios Goumas²

Christina Giannoula 1

ABSTRACT

Sparse Convolution (SpC) powers 3D point cloud networks widely used in autonomous driving and AR/VR. SpC builds a kernel map that stores mappings between input voxel coordinates, output coordinates, and weight offsets, then uses this map to compute feature vectors for output coordinates. Our work identifies three key properties of voxel coordinates: they are integer-valued, bounded within a limited spatial range, and geometrically continuous—neighboring voxels on the same object surface are highly likely to exist at small spatial offsets from each other. Prior SpC engines do not fully exploit these properties and suffer from high pre-processing and post-processing overheads during kernel map construction. To address this, we design Spira, the first voxel-property-aware SpC engine for GPUs. Spira proposes: (i) a high-performance one-shot search algorithm that builds the kernel map with *no* preprocessing and high memory locality, (ii) an effective packed-native processing scheme that accesses packed voxel coordinates at low cost, (iii) a flexible dual-dataflow execution mechanism that efficiently computes output feature vectors by adapting to layer characteristics, and (iv) a network-wide parallelization strategy that builds kernel maps for all SpC layers concurrently at network start. Our evaluation shows that Spira significantly outperforms prior SpC engines by 1.71× on average and up to 2.31× for end-to-end inference, and by 2.13× on average and up to 3.32× for layer-wise execution across diverse layer configurations.

1 Introduction

Point cloud data has become increasingly used in various important applications, including autonomous driving (Zermas et al., 2017), robotics (Kim et al., 2018), augmented/virtual reality (Wirth et al., 2019), and drones (Zheng et al., 2020). Light detection and ranging (LiDAR) sensors on autonomous vehicles, drones, and mobile devices generate point cloud data that are processed by point cloud networks. Voxel-based point cloud networks achieve state-of-the-art accuracy (Hong et al., 2023) in vision tasks such as object detection (Yin et al., 2021) and segmentation (Zhu et al., 2021) by processing voxelized point clouds (referred to as voxel data)—raw point cloud data have been quantized into a discrete 3D grid of small cubes (voxels).

Unlike 2D images, 3D point clouds are extremely sparse, typically occupying less than 0.01% of their bounding volume (Lin et al., 2021). Sparse Convolution (**SpC**) is therefore the dominant computational kernel in voxel-based point cloud networks, consisting of two steps. 1) The **voxel indexing** step generates the output voxel coordinates, and the mappings between the input coordinates, output coordinates

and the weight offsets. Voxel indexing finds and stores these mappings in a table called **kernel map**, performing lookup operations (**searches**) on a query data structure containing the voxel coordinates. To accomplish this, SpC engines include a **pre-processing** phase that organizes coordinates in a query data structure, and may include a **post-processing** phase that rearranges and filters the kernel map for the subsequent feature computation step. 2) The **feature computation** step produces the feature vectors (actual convolution output) for the output coordinates based on the kernel map mappings. This step is parallelized across thread blocks using one of two dataflow approaches: **output-stationary** or **weight-stationary**, explained in § 2.2. Prior work (Tang et al., 2023) shows both dataflows are necessary, since each performs best under different layer characteristics.

In this work, we extensively characterize voxel data processed in SpC and analyze prior state-of-the-art SpC engines. We identify two key limitations (§ 3): prior works (Tang et al., 2022; 2023; Yang et al., 2024; Spconv2, 2022; Hong et al., 2023; Choy et al., 2019) incur non-negligible performance overheads in the pre-processing and post-processing phases of voxel indexing, and lack efficient support for both output- and weight-stationary dataflows required for feature computation. We also identify three key properties of voxel data. First, voxel coordinates are integer-valued, as each voxel point is a triplet of values representing a *discrete* voxel (cube) in a 3D grid. Second, they are spatially

¹Max Planck Institute for Software Systems (MPI-SWS) ²National Technical University of Athens (NTUA). Correspondence to: Christina Giannoula <cgiannoula@mpi-sws.org>.

bounded within a limited value range, since they represent a *finite* 3D grid, the exact size of which depends on the captured environment of each application (§ 4). Third, they are geometrically continuous, as they represent continuous object surfaces: neighboring voxel coordinates on the same object are highly likely to exist at small offset displacements from each other. Prior SpC engines do not fully exploit these properties. We demonstrate that leveraging these properties can significantly reduce computation and data access costs in SpC, leading to substantial performance improvements.

To this end, we design Spira, the first SpC engine that comprehensively exploits voxel data structural properties to accelerate performance. Spira relies on four key ideas. First, we design a one-shot search algorithm that completely eliminates the pre-processing phase in voxel indexing, and performs fast localized searches by exploiting the integer-valued property, thereby reducing expensive irregular lookup operations. Second, we pack each voxel point triplet into a single integer value by exploiting the spatially bounded property of voxel data, and design packed-native kernels that *directly* perform voxel indexing on packed data, eliminating unpacking/repacking overheads and reducing compute and data access costs. Third, we propose an adaptive hybrid dataflow scheme for feature computation that selects output-stationary, weight-stationary dataflow or hybrid combinations of both dataflows based on kernel map density patterns identified using the geometric continuity property of voxel data. This approach improves feature computation performance by adapting execution dataflow to both layer characteristics and kernel map densities. Fourth, we identify that voxel indexing steps across SpC layers have no dependencies between them or with other operators throughout the network, and we execute all voxel indexing steps concurrently at the network start across multiple GPU SMs, thus improving resource utilization and execution parallelism.

We extensively evaluate Spira using a wide variety of 3D point cloud networks, real-world datasets from indoor and outdoor scenes, and three GPU architectures, demonstrating that Spira significantly outperforms prior SpC engines. In end-to-end point cloud inference, Spira improves performance by $1.61 \times$, $1.86 \times$, and $1.81 \times$ on average and up to $2.15 \times$, $2.19 \times$, and $2.61 \times$ over prior state-of-the-art engines on RTX 3090, A100, and Quadro RTX 5000 GPUs, respectively. At the SpC layer level, Spira achieves $2.13 \times$ speedup on average and up to $3.32 \times$ speedup over prior work across various layer configurations. We will open-source Spira upon acceptance to enable further research and practical applications. Overall, we make the following contributions:

- We identify important structural properties of voxel data and propose Spira, the first voxel-property-aware SpC engine for GPU architectures.
- We propose a one-shot search algorithm that performs lo-

calized searches and eliminates pre-processing, and design packed-native voxel indexing that exploits voxel properties to reduce compute and data access costs. We propose network-wide voxel indexing that executes all layers' voxel indexing steps concurrently, and design an adaptive hybrid dataflow scheme that adapts feature computation dataflow to layer characteristics and kernel map densities.

 We evaluate Spira across diverse real-world datasets, point cloud networks and GPUs, demonstrating significant performance improvements over state-of-the-art SpC engines.
We will publicly release Spira for further research.

2 BACKGROUND

2.1 Sparse Convolution (SpC) Definition

A point cloud is an unordered set of 3D points, representing locations on the surface of an object or within a scene. Unlike images, point clouds are irregularly distributed and spatially sparse, making standard convolutional neural networks inefficient (Wu et al., 2019). To enable convolutional processing, point clouds are often voxelized by discretizing the 3D space into a regular grid of small cubes (voxels). A voxelized point cloud (henceforth referred as voxel **data**) can be represented as a set of tuples $\{(\mathbf{v}_i, \mathbf{f}_i)\}$, where $\mathbf{v}_i \in \mathbb{Z}^3$ denotes the quantized coordinate of the i-th voxel in the 3D-grid space, and $\mathbf{f}_i \in \mathbb{R}^C$ is its corresponding feature vector. The quantization from continuous to discrete space is performed as $\mathbf{v}_i = \lfloor \mathbf{p}_i^{(\mathrm{raw})}/\mathbf{g} \rfloor$, where $\mathbf{p}_i^{(\mathrm{raw})} \in \mathbb{R}^3$ are the original continuous coordinates of the i-th point and $\mathbf{g} \in \mathbb{R}^3$ the grid size vector that determines the spatial resolution, both typically measured in meters.

Sparse Convolution (SpC) is the dominant operation in voxel-based point cloud networks. It takes as input voxel data p with coordinates \mathbf{V}_p and its output q is also a voxel data with coordinates \mathbf{V}_q , controlled by a stride parameter (Choy et al., 2019). Given input stride s_p and layer stride s_l , the output stride is $s_q = s_p \times s_l$. When $s_l = 1$, the output coordinates coincide with the input, $\mathbf{V}_q = \mathbf{V}_p$ (submanifold convolution), which comprises the majority of layers in point cloud networks. When $s_l > 1$, downsampling is applied for the output coordinates as $\mathbf{V}_q = \lfloor \frac{\mathbf{V}_p}{s_q} \rfloor \times s_q(1)$, keeping only the unique values. Downsampling typically uses $s_l = 2$, so after m downsamplings, the output stride becomes $s_q = 2^m$ (Lin et al., 2021).

For the input features $F_p \in \mathbb{R}^{|\mathbf{V}_p| \times \mathbf{C_{in}}}$ and the output features $F_q \in \mathbb{R}^{|\mathbf{V}_q| \times \mathbf{C_{out}}}$, $\mathbf{C_{in}}$ and $\mathbf{C_{out}}$ are the input and output channel sizes, respectively. The output feature vector \mathbf{f}_i^q of the i-th output coordinate \mathbf{q}_i is computed over all weight offsets $\boldsymbol{\delta}_k$ and input coordinates \mathbf{p}_j that satisfy the condition $\mathbf{p}_j = \mathbf{q}_i + \boldsymbol{\delta}_k$, as follows:

$$\mathbf{f}_{i}^{q} = \sum_{\boldsymbol{\delta}_{k} \in \Delta(K, s_{p})} \sum_{\mathbf{p}_{j} \in \mathbf{V}_{p}} \mathbf{1}_{\mathbf{p}_{j} = \mathbf{q}_{i} + \boldsymbol{\delta}_{k}} \mathbf{f}_{j}^{p} \mathbf{W}_{\boldsymbol{\delta}_{k}}, \quad (\mathbf{q}_{i} \in \mathbf{V}_{q})(2)$$

where $\Delta(K, s_p)$ is the set of K^3 weight offsets of kernel size K and input stride s_p (e.g., $\Delta(5,2) = \{-4, -2, 0, 2, 4\}^3$), δ_k is the k-th weight offset, \mathbf{f}_j^p is the feature vector of the input coordinate \mathbf{p}_j , $\mathbf{W}_{\delta_k} \in \mathbb{R}^{\mathbf{C_{in}} \times \mathbf{C_{out}}}$ is the weight corresponding to offset δ_k , and $\mathbf{1}_{\mathbf{p}_j = \mathbf{q}_i + \delta_k}$ is the indicator function for the condition $\mathbf{p}_j = \mathbf{q}_i + \delta_k$.

2.2 The Execution Steps of SpC

The execution of a SpC layer can be split into two steps: 1) Voxel Indexing Step. It consists of the downsampling and mapping parts. Downsampling is performed in SpC layers with $s_l > 1$, and generates output voxel coordinates according to Eq. 1 through element-wise rounding and duplicate removal. State-of-the-art downsampling schemes sort coordinates to identify and remove duplicates. Mapping builds a $|\mathbf{V}_q| \times K^3$ matrix M, called the **kernel map**, that stores the mappings between the input coordinates, the output coordinates and the weight offsets. These mappings guide the feature vector computation for output coordinates according to Eq. 2, as described in the feature computation step. SpC engines build the kernel map in three phases: (i) organize coordinates in a query data structure (pre-processing phase), (ii) perform lookup operations (search phase) of the queries $q_i + \delta_k$ for each output coordinate q_i and each weight offset δ_k : if the query $q_i + \delta_k$ matches an input coordinate p_i in the query data structure, then M[i, k] = j, otherwise M[i, k] = -1 (invalid entry), (iii) filter invalid entries (-1) and rearrange the kernel map (**post-processing** phase), if needed. Thus, mapping has preprocessing kernels that build the query data structure, search operations and potentially post-processing kernels that rearrange and filter the kernel map for feature computation.

2) Feature Computation Step. It computes the feature vectors of output coordinates according to Eq. 2. Two dataflow types exist, shown in Fig. 1. I) The Output-**Stationary** dataflow (Fig. 1 top) distributes the output coordinates q_i across thread blocks: each thread block computes feature vectors associated with all weight offsets $\delta_{\mathbf{k}}$ for a chunk of the output coordinates. Although thread blocks directly produce the final output feature vectors \mathbf{f}_{i}^{q} , they perform unnecessary zero-valued multiplications, since the kernel map is *not* filtered to remove invalid entries. II) The Weight-Stationary dataflow (Fig. 1 bottom) requires the kernel map to be transposed relative to outputstationary format to enable coalesced memory writes among threads within a thread block, and **filtered** from invalid entries. It distributes the weight offsets across thread blocks: each thread block is assigned a weight offset $\delta_{\mathbf{k}}$ and computes partial sums for the output feature vectors \mathbf{f}_i^q over a chunk of valid input-output coordinate pairs. Although this dataflow eliminates unnecessary computations, thread blocks produce partial results for same output feature vectors, which are merged using expensive atomic instructions

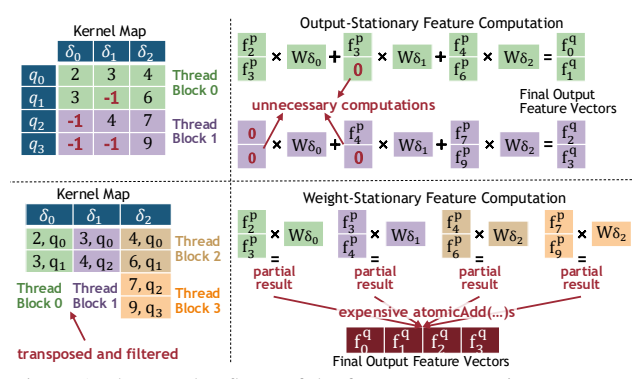


Figure 1. The two dataflows of the feature computation step.

(e.g., atomicAdd) to obtain the final output vectors. Prior work (Tang et al., 2023) shows that **both** dataflows are needed to achieve optimal performance across varying layer configurations and kernel map densities.

3 EXISTING SPC ENGINES

Prior works improve SpC performance on GPUs. MinkowskiEngine (Choy et al., 2019) is the first opensource library providing a generalized sparse convolution for point clouds. SpConv2 (Spconv2, 2022) library introduced the output-stationary dataflow. TorchSparse (Tang et al., 2022) optimized the weight-stationary dataflow, while PCEngine (Hong et al., 2023) further improved it by dynamically adapting between two weight-stationary variants. TorchSparse++ (Tang et al., 2023) supports both dataflows, and its latest public source code (GitHub, 2025) integrates optimizations from both SpConv2 and PCEngine, achieving significant performance improvements over these prior works. Minuet (Yang et al., 2024) proposes a binary-searchbased algorithm for kernel map construction, but only supports weight-stationary dataflow. While Minuet outperforms MinkowskiEngine and TorchSparse, it does not compare with TorchSparse++. TorchSparse++ (latest public code) and Minuet are the two best-performing engines; thus, we focus our evaluation on these state-of-the-art baselines.

Fig. 2 shows the performance breakdown in two submanifold layers of TorchSparse++ output- and weight-stationary dataflows, Minuet and Spira with both dataflows and its own hybrid dataflow. Numbers above each bar show the speedup of each engine over TorchSparse++ output-stationary.

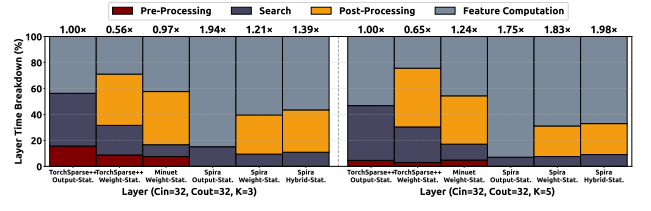


Figure 2. Layer time breakdown using various SpC engines. Numbers on bars are speedup over TorchSparse++ output-stationary.

We make two observations. First, although Minuet achieves

4.31× faster search time than TorchSparse++, it incurs noticeable pre-processing overhead, e.g., in the first layer (left), pre-processing time is *nearly equal* to search time. Instead, Spira *completely* eliminates pre-processing, and achieves $7.83\times$ and $1.82\times$ faster search time than TorchSparse++ and Minuet, respectively. Second, TorchSparse++ and Minuet have limited dataflow support. Minuet supports only weight-stationary, while TorchSparse++ incurs significant post-processing costs in weight-stationary by transposing the *entire* kernel map to exploit coalesced memory writes. Spira efficiently supports both dataflows: e.g., Spira outputstationary performs best in the first layer (left), while Spira weight-stationary significantly outperforms prior engines in the second layer (right), having 5.42× lower post-processing overhead than TorchSparse++. Additionally, Spira enables hybrid dual-dataflow execution that exploits voxel data properties to further accelerate feature computation. In the second layer (right), Spira with hybrid dataflow is 1.98× and 1.60× faster than TorchSparse++ and Minuet, respectively.

4 IDENTIFIED VOXEL DATA PROPERTIES

We comprehensively analyze the voxel coordinate data in SpC layers, and we identify three key structural properties.

- (1) Integer Property: Voxel coordinates are integer-valued. Raw point cloud coordinates are quantized to a discrete 3D grid with grid size vector g (§ 2.1), resulting in integer coordinates (v_x, v_y, v_z) along each axis (x, y, z). Moreover, Eq. 1 explains that when voxel coordinates are downsampled with stride s > 1, they are rounded to integer multiples of s.
- (2) Bounded Property: Voxel coordinates are bounded within a limited value range. Point cloud data, indoor and outdoor scenes, is spatially constrained by the capture environment and sensor capabilities, having a range of (R_x, R_y, R_z) (e.g., expanding through R_x meters in the x-axis). In indoor scenes, the x and y axes represent the horizontal room dimensions, thus being inherently bounded, while the z axis represents the vertical room height, inherently bounded by the floor-to-ceiling distance. In outdoor scenarios (e.g., autonomous driving), the x and y axes correspond to the forward and lateral directions, bounded by the sensor's capture range (horizontal field of view). For example, in Waymo dataset (Sun et al., 2019), the horizontal LiDAR radius is ~75 meters, yielding $R_x, R_y \leq 150$ meters. The vertical z axis range R_z is typically cropped to a few meters (Yin et al., 2021) to focus on the height of relevant nearby objects. Since raw point cloud coordinates are bounded by a spatial range, the corresponding quantized integer voxel coordinates are also bounded by spatial range $\left(\left\lfloor\frac{R_x}{g_x}\right\rfloor, \left\lfloor\frac{R_y}{g_y}\right\rfloor, \left\lfloor\frac{R_z}{g_z}\right\rfloor\right)$, where $g=(g_x,g_y,g_z)$ is the grid size vector, resulting in a finite, well-defined 3D grid whose exact extent depends on the application.

(3) L1-Norm Density Property: In submanifold convolution, kernel map columns for weight offsets with smaller L1 norms ¹ consistently exhibit higher density than those with larger L1 norms, reflecting the geometric continuity of object surfaces captured by voxel data. Voxel coordinates capture continuous object surfaces rather than randomly scattered points. When a voxel exists at position (v_x, v_y, v_z) on a voxelized object surface, its immediate neighbors at small L1-norm offsets (± 1 in x, y, or z axis) are likely to be occupied, belonging to the *same* surface. In contrast, large L1-norm offsets that shift coordinates across multiple axes (e.g., simultaneously along x, y, and z) by larger displacements are highly likely to reach empty space. For example, Fig. 3 a) shows a voxelized wall with the green voxel (cube) annotated. The blue voxel that has been shifted by (0,1,1)(small L1-norm of 2) from the green voxel, belongs to the same wall surface, while the red voxel, shifted by (2,2,2)(larger L1-norm of 6), corresponds to empty space (air).

This geometric property has important implications for submanifold layers—which constitute over 70% of layers in state-of-the-art point cloud networks-where output coordinates are identical to input coordinates. We comprehensively examine *hundreds* of voxel point clouds from publicly available indoor and outdoor datasets and observe that in submanifold layers, kernel map columns for weight offsets with small L1-norms consistently exhibit higher density than columns for larger L1-norms. This occurs because voxel coordinates of the same object surface differ by small L1-norms (small offset displacements), whereas coordinates differing by larger L1-norms (larger offset displacements) typically correspond to empty space. In a SpC layer with input stride s_p , the L1-norm of weight offsets takes values from 0 up to L1NormMax = $\frac{3(K-1)}{2} \times s_p$, in steps of s_p . Fig. 3 b) shows the average density of kernel map columns for weight offsets grouped by L1 norm (0 to 6) across three datasets in a layer with K=5 (125 total weight offsets) and s_p =1. The column for weight offset (0,0,0) exhibits 100% density, because, by definition of submanifold convolution, each output voxel coordinate maps to itself as an input coordinate—ensuring a *non-empty* input coordinate exists for every output coordinate. Columns for weight offsets with L1-norm of 1 average 39.4% density across datasets, while those with L1-norm of 6 average only 5.4% density.

5 SPIRA DESIGN

5.1 Overview

Spira is the first voxel-property-aware SpC engine that integrates fast mapping search, reduces coordinate access costs, improves parallelism in voxel indexing, and supports flexible hybrid dataflow processing. Spira has four key ideas:

¹L1 norm of weight offset $\delta = (\delta_x, \delta_y, \delta_z)$ is $|\delta_x| + |\delta_y| + |\delta_z|$.

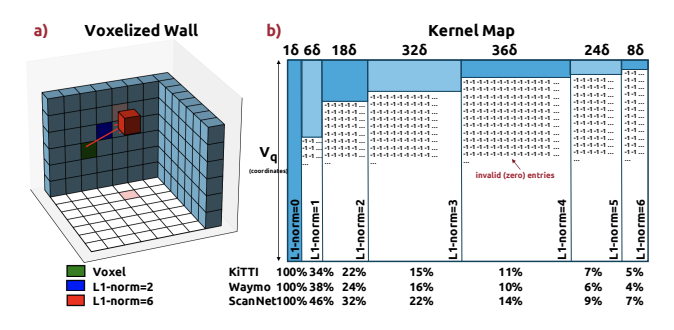


Figure 3. a) A voxelized wall surface. b) In a submanifold layer with K=5, the average density of kernel map columns for weight offsets grouped by their L1-norm for three different datasets.

- 1. One-Shot Z-Delta Search Mapping. We design a one-shot search algorithm that builds the kernel map with *no* pre-processing phase. By intelligently partitioning weight offsets into K^2 groups of K offsets each, we perform only one binary search per group to resolve the first query, then we use fast localized search to resolve the remaining K-1 queries of that group. This approach significantly reduces memory accesses and computational cost.
- **2. Packed-Native Voxel Indexing.** Leveraging the bounded property, we pack three coordinate values into a single (32-bit or 64-bit) integer, and propose packed-native voxel indexing that *directly* processes packed data, completely eliminating unpacking/repacking and reducing data access costs.
- 3. Adaptive Hybrid-Dataflow Feature Computation. We exploit the L1-norm density property in feature computation and propose a flexible hybrid dataflow scheme where different weight offsets in kernel map can be processed with either output- or weight-stationary way. This approach spans the full dataflow range, from single-dataflow executions to flexible hybrid combinations. This way we find the optimal trade-off between unnecessary computations and expensive atomic operations for each layer's specific configuration.
- **4. Network-Wide Voxel Indexing.** Via detailed network analysis, we find voxel indexing kernels have *no* dependencies, thus we execute them concurrently at the network start across multiple GPU SMs to improve execution parallelism.

5.2 One-Shot Z-Delta Search Mapping

The **goal** of our mapping search scheme is to achieve (i) minimal pre-processing overhead and (ii) fast search lookup operations for the queries $\mathbf{q_i} + \delta_{\mathbf{k}}$ ($\mathbf{q_i}$ output coordinate and $\delta_{\mathbf{k}}$ weight offset). Spira's algorithm *completely* eliminates pre-processing leveraging the following key observation.

Key Observation: When input voxel coordinates of the first SpC layer of a network are lexicographically sorted, all SpC layers maintain sorted coordinates throughout the network. In submanifold layers $(s_l = 1)$, output coordinates are identical to input coordinates, directly preserving the sorted order. In downsampling layers $(s_l > 1)$, the fastest downsampling schemes of state-of-the-art SpC engines extract

unique output coordinates by rounding input coordinates, and sorting the rounded results to remove duplicates—a process that inherently produces sorted output coordinates V_q . Since each layer's output become the next layer's input, sorting propagates naturally through the network. Thus, sorting coordinates once at the first layer guarantees sorted coordinates throughout all layers.

Our **one-shot** search algorithm eliminates the preprocessing by operating directly on the default coordinate arrangement: input and output coordinates of all network layers stored in separate sorted arrays, requiring only a single sort in the first layer's input coordinates. To search for queries $\mathbf{q_i} + \delta_{\mathbf{k}}$ in each layer's input coordinate array, we generate these queries *on-the-fly* by adding the current weight offset $\delta_{\mathbf{k}}$ to each sorted output coordinate $\mathbf{q_i}$.

A simple binary search algorithm can exploit this sorted arrangement without pre-processing: parallel threads generate queries $\mathbf{q_i} + \boldsymbol{\delta_k}$ on-the-fly and perform binary search on the input coordinate array to find mappings between input coordinates, output coordinates and weight offsets. This simple algorithm performs $|V_q| \times K^3$ independent binary searches—one per generated query. However, despite exhibiting high temporal data locality when searching sorted queries (Yang et al., 2024), performing one full binary search per query in the entire input coordinate array in global memory remains expensive due to the large number of memory accesses and high computational complexity.

Spira leverages the **Integer Property** of voxel data to reduce computational complexity, while maintaining a one-shot design without pre-processing. Fig. 4 presents our proposed **z-delta search** algorithm in a layer with kernel size K=3 and input stride $s_p=1$. We group the K^3 weight offsets δ in K^2 groups of K offsets each, where offsets within a group have identical x and y values and consecutive z values, e.g., the offsets (-1, -1, -1), (-1, -1, 0), (-1, -1, 1) form group 0. We distribute the sorted output coordinates and weight offset groups among parallel threads: each thread processes all the K queries from $q_i + \delta_i$ to $q_i + \delta_{i+K-1}$ for a single coordinate q_i and weight offset group. This grouping ensures the K query coordinates range from (x, y, z) to $(x, y, z + (K-1) \times s_p)$ —sharing identical x and y values and having consecutive z values increasing by s_p . For instance, for output coordinate (50,4,5), thread 0 processes weight offset group 0 and generates K=3 queries (49,3,4), (49,3,5) and (49,3,6) with identical x and y values and z values increasing by $s_p=1$.

Key Observation: For a thread processing the K queries from (x, y, z) to $(x, y, z + (K-1) \times s_p)$ for the same weight offset group, the **sorted** and **integer-based** nature of the input coordinate array ensures that consecutive queries (x, y, z) and $(x, y, z + s_p)$, if they exist, must occupy consecutive positions in the array. There cannot be three coordinates

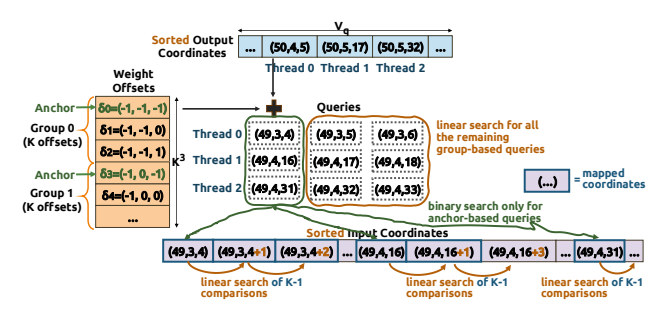


Figure 4. Spira's one-shot z-delta search algorithm.

 $(x,y,z),(x,y,z'),(x,y,z+s_p)$ where $z < z' < z+s_p$, in the input coordinate array. This follows directly from the **Integer Property** and SpC definition: since input coordinates are integer and multiples of stride s_p and are lexicographically sorted in input array, **no** coordinate can exist between (x,y,z) and $(x,y,z+s_p)$, with the identical x and y values (input coordinates must differ by some multiples of s_p).

Our z-delta search algorithm (Fig. 4) exploits this key observation to reduce computational complexity, and improve memory locality. For $|V_q|$ output coordinates and K^3 weight offsets, z-delta search performs only $|V_q| \times K^2$ binary searches. For each weight offset group, the offset with the smallest z-value serves as the anchor (e.g., $\delta_0 = (-1, -1, -1)$ is the anchor in group 0). For the K queries generated from the same weight offset group, we perform binary search in the input coordinate array **only** for the anchor-based query (e.g., (49,3,4) query for group 0). The binary search returns the position the matched input coordinate-or, if no match exists, the next larger coordinate. We resolve the remaining K-1 queries (e.g., (49,3,5) and (49,3,6) queries for group 0) via a quick localized linear search starting from this position: the local linear search checks at most K-1 consecutive positions in the input array to look for potential matchings for the remaining K-1queries. Since these positions are contiguous in memory, the localized linear search achieves optimal cache efficiency with minimal data access latency. Overall, our z-delta search algorithm enables one-shot kernel map construction with low computational cost and high data locality, significantly reducing expensive global memory accesses.

5.3 Packed-Native Voxel Indexing

Prior SpC engines use 32 bits for *each* of the three voxel coordinates of a triplet. Instead, Spira leverages the **Bounded Property** to represent each integer coordinate with fewer bits and pack all three coordinates into a *single* integer value.

For many real-world applications (e.g., automotive, robotics), packing all three coordinates into a single 32-bit value is sufficient. For example, outdoor scenes using LiDAR sensors with a total capture range R_x and R_y of up to 400 meters, requiring 20 meters for vertical range R_z and quantized with grid size of 0.1 meters can be represented

using 12, 12, 8 bits for v_x , v_y and v_z coordinates, respectively. For highly demanding applications, Spira can pack voxel coordinates into a single 64-bit value (See Fig.Fig. 7). Note that 64-bit packing for the voxel coordinate triplet is sufficient for all current real-world SpC applications: 64-bit packing can represent scenes with ranges R_x , R_u , R_z up to several kilometers and satisfying spatial resolutions of the grid size vector g up to millimeters, which provides the maximum accuracy that today's 3D sensors can support to v_z) as one single value: each v_i integer value is within an integer range of $\lfloor \frac{R_i}{g_i} \rfloor$, thus the necessary bits to express it are at most $b_i = \log(\lfloor \frac{R_i}{g_i} \rfloor)$. The first b_x most significant bits for x, next b_y bits for y and the remaining b_z bits for z. In § 6, we use 12, 12, and 8 bits for v_x , v_y and v_z , respectively. However, the bit allocation is flexible and can be easily configured.

The **key challenge** with packed coordinates is how to avoid unpacking and repacking operations in the SpC voxel indexing kernels (feature computation does not use voxel coordinates). Spira enables **packed-native voxel indexing** in both downsampling and mapping kernels, *completely* eliminating any unpacking/repacking, thus the only packing required for voxel data is performed once in the initial coordinates.

In downsampling, rounding each packed input coordinate with the output stride $s_q = 2^m$ can be efficiently performed by bitwise adding two 32-bit values: the packed coordinate $packed(p_j)$ and the $mask = \underbrace{11\cdots1}_{b_x-m}\underbrace{00\cdots0}_{m}\underbrace{11\cdots1}_{b_y-m}\underbrace{00\cdots0}_{m}\underbrace{11\cdots1}_{b_z-m}\underbrace{00\cdots0}_{m}$. Downsampling also requires sorting packed coordinates to remove duplicates. Notably, sorting directly in packed format inherently preserves lexicographic order: $p_i > p_j \Leftrightarrow packed(p_i) > packed(p_j)$. Therefore, we can directly sort the packed coordinates without unpacking.

In mapping, we apply to the output coordinates q_i and weight offsets δ_k exactly the same packing format as used in input coordinates, representing each as a single packed value. We leverage the property that $packed(q_i) + packed(\delta_k) = packed(q_i + \delta_k)$, which allows us to directly generate queries $q_i + \delta_k$ as $packed(q_i) + packed(\delta_k)$ represented in the same packed format. This eliminates the need to unpack the $packed(q_i)$, add weight offset to generate $q_i + \delta_k$, and repack the result. The lookup searchs of mapping can be also directly performed using packed queries , as packed format preserves lexicographic order: $(q_i + \delta_k) > p_j \Leftrightarrow packed(q_i) + packed(\delta_k) > packed(p_j)$.

Spira's packed-native voxel indexing provides four performance benefits over prior works: (i) memory footprint for voxel coordinates is lower (e.g., 3× lower for 32-bit packing), (ii) memory reads and writes for voxel coordinates are faster thanks to fewer global memory accesses, (iii) lexico-

graphic sorting during downsampling is faster when sorting a single (32-bit or 64-bit) value compared to sorting three separate (32-bit) values, and (iv) lexicographic comparisons for lookup operations during mapping are faster—a single comparison of a packed coordinate value is more faster than three separate comparisons of individual coordinates.

5.4 Adaptive Hybrid-Dataflow Feature Computation

Output-stationary and weight-stationary dataflows each perform best under different kernel map densities and SpC layer characteristics. When the kernel map is relatively dense (fewer invalid entries), output-stationary dataflow performs better by avoiding kernel map filtering and eliminating expensive atomic operations during feature computation. Instead, when the kernel map is relatively sparse (large number of invalid entries), weight-stationary dataflow is more efficient by skipping numerous zero-valued multiplications.

In submanifold layers—which typically constitute $\sim 70\%$ of SpC layers in state-of-the-art point cloud networks—the **L1-Norm Density Property** states that kernel map columns corresponding to weight offsets with smaller L1 norms consistently exhibit higher density than those with larger L1 norms. For example, in SpC layers with $K \geq 5$, most weight offset columns are up to $10\times$ sparser than a small subset of significantly denser columns. This property implies that using a single dataflow (either output-stationary or weight-stationary) for feature computation is suboptimal. Instead, a hybrid dual-dataflow approach that selects the appropriate dataflow for each weight offset based on its density could achieve better performance.

To address this, Spira's feature computation scheme (i) supports the full dataflow spectrum, including single-dataflow execution (all weight offsets processed using one dataflow) and hybrid dual-dataflow execution (different weight offset subsets processed using different dataflows), and (ii) minimizes post-processing costs for kernel map rearrangement required by each dataflow. Fig. 5 provides an overview of Spira's adaptive hybrid dataflow for feature computation.

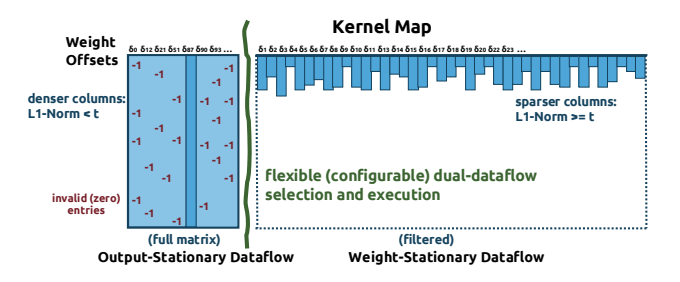


Figure 5. Spira's adaptive hybrid-dataflow feature computation.

We track the density of all kernel map weight offsets in and select the appropriate dataflow for each weight offset by classifying them as *dense* or *sparse* using a configurable threshold t: weight offsets with L1-norm < t are

are classified as dense and processed with output-stationary dataflow, and weight offsets with L1-norm $\geq t$ are classified as sparse and processed with weight-stationary dataflow. When t=L1NormMax+1, all columns are considered dense, degenerating to full output-stationary execution. When t=0, all columns are considered sparse, degenerating to full weight-stationary execution.

Spira tunes the threshold value t for each SpC layer using the same general tuning approach as prior state-of-the-art works (Yang et al., 2024; Tang et al., 2023; Hong et al., 2023). We sample a few point clouds from the dataset and measure kernel map built time and feature computation latency for different (integer) t values, then select the t value that minimizes total latency. Note that this is a *one-time* tuning step performed only once before inference, having negligible overhead. The **key challenge** is how to fully support adaptive hybrid dataflow executions with low post-processing overheads in voxel indexing.

Output-stationary dataflow requires the kernel map to be in $|V_q| \times K^3$ layout, while weight-stationary requires it transposed (§ 2.2) to $K^3 \times |V_q|$ layout (also filtered from invalid indices). These layouts enable memory coalescing in kernel map construction: adjacent threads within a thread block write to adjacent memory locations, maximizing memory bandwidth utilization. Similarly, hybrid dualdataflow with K_{dense} dense weight offsets and K_{sparse} sparse weight offsets where $K_{dense}+K_{sparse}=K^3$, requires two kernel map submatrices: one of $|V_q| \times K_{dense}$ layout for output-stationary and another of $K_{sparse} \times |V_q|$ layout (also filtered) for weight-stationary, both enabling memory coalescing. These different layout requirements could incur high post-processing overheads in voxel indexing, as the entire kernel map must be rearranged into the appropriate layout for each dataflow, thus potentially negating the performance benefits of hybrid dual-dataflow execution.

Spira achieves low post-processing time across all three dataflow scenarios (Fig. 6) by optimizing how queries are distributed across parallel threads within a thread block. I) Full output-stationary t=L1NormMax+1 (Fig. 6a): Spira has **no** post-processing (zero). Our z-delta search distributes different weight offsets δ_i for the same output coordinate qi across multiple threads within a thread block, enabling coalesced memory writes that directly produce the required $|V_a| \times K^3$ layout. II) Full weight-stationary t=0 (Fig. 6b): Spira has post-processing *only* for filtering invalid entries (no transposition needed). Our z-delta search distributes different output coordinates q; for the same weight offset δ_i across threads within a thread block, enabling coalesced memory writes that directly produce the required $K^3 \times |V_q|$ layout. III) Hybrid dual-dataflow $0 < t \le L1$ NormMax, where t is multiple of s_p (Fig. 6c): Our z-delta follows the weight-stationary parallelism scheme (distributing different

output coordinates $\mathbf{q_i}$ for the same weight offset $\delta_{\mathbf{j}}$ across threads). We employ an auxiliary buffer of size K^3 to help us classify weight offsets as *dense* and *sparse* and partition the kernel map into two submatrices: one with $K_{dense} \times |V_q|$ layout storing all dense weight offset rows contiguously, and another with $K_{sparse} \times |V_q|$ layout storing all sparse weight offset rows contiguously. Post-processing then transposes *only* the dense submatrix to produce the required $|V_q| \times K_{dense}$ layout, and filters *only* the sparse submatrix to remove invalid entries. The post-processing time in hybrid dual-dataflow is minimal and comparable to that of the full weight-stationary dataflow.

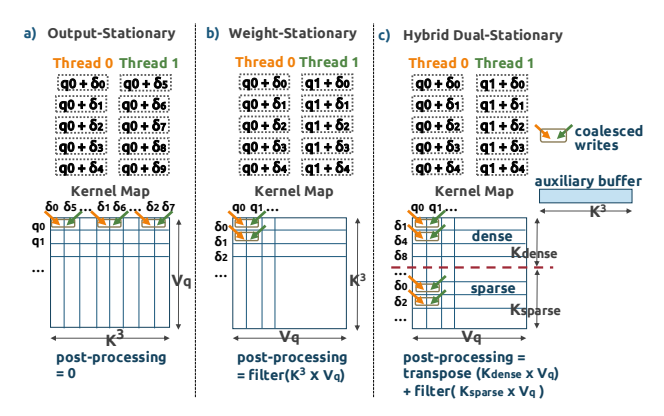


Figure 6. Spira's post-processing in three dataflow scenarios.

In submanifold layers, Spira further reduces post-processing time for weight-stationary dataflow and weight-stationary submatrix in hybrid dual-dataflow by exploiting a symmetry property from prior work (Tang et al., 2022): weight offsets $\delta_l=(b,c,d)$ and $\delta_n=(-b,-c,-d)$ are symmetric, i.e., if M[i,l]=j>0 in the kernel map, then M[j,n]=i>0. Weight-stationary feature computation, where each thread block operates on a fixed weight offset, compute outputs features for symmetric weight offset pairs by reading only the first half of the kernel map. Thus, only half of kernel map is stored and filtered, reducing post-processing time.

5.5 Network-Wide Voxel Indexing

We carefully examine point cloud network operators and make the following **Key Observation**: The voxel indexing step of a SpC layer has **no** true data dependencies with voxel indexing or feature computation steps of other layers. Our profiling also shows that voxel indexing incurs low GPU SM utilization, as it performs only lightweight comparisons.

Voxel indexing step includes downsampling to generate output coordinates, and mapping, that uses them to construct the kernel map needed in feature computation step. Typical downsampling for layer i is performed recursively as $V_i = \lfloor \frac{V_{i-1}}{2^i} \rfloor \times 2^i$ using the voxel coordinates V_{i-1} from the previous downsampling layer. However, we find that this recursive formula can be transformed into a closed-form

expression using only the initial input coordinates V_0 :

$$V_{i} = \left\lfloor \frac{V_{i-1}}{2^{i}} \right\rfloor 2^{i} = \left\lfloor \frac{\left\lfloor \frac{V_{i-2}}{2^{i-1}} \right\rfloor 2^{i-1}}{2^{i}} \right\rfloor 2^{i}$$
$$= \left\lfloor \frac{V_{i-2}}{2^{i}} \right\rfloor 2^{i} = \dots = \left\lfloor \frac{V_{0}}{2^{i}} \right\rfloor 2^{i} \tag{1}$$

Thus, according to Eq.1, downsampling kernels of different layers have *no* true dependencies with each other: voxel coordinates of layer i can be *directly* extracted from the initial coordinates V_0 . Moreover, mapping kernels are also mutually *independent*, since each mapping kernel only requires its associated layer's downsampled coordinates to build the kernel map consumed by subsequent feature computation.

Spira enables **network-wide voxel indexing** by executing voxel indexing steps for all layers in parallel at the network start via a two-phase process. First, all downsampling kernels across all layers are executed concurrently using CUDA streams distributed across multiple GPU SMs, generating coordinate sets for their corresponding mapping kernels. Second, all mapping kernels are executed concurrently, again using streams across multiple SMs to produce kernel maps for all layers. These kernel maps are stored in global memory and consumed by their corresponding feature computation steps as inference progresses. Kernel maps storage requires on average $\sim 40 \text{MB}$ of global memory—affordable even for edge GPUs—and this memory is deallocated progressively as each kernel map is no longer needed. Submanifold layers with weight-stationary dataflow store only half the kernel map (See 5.4), further reducing the memory footprint. Spira's network-wide voxel indexing improves execution parallelism and GPU utilization.

6 EVALUATION

6.1 Evaluation Methodology

Hardware Systems/GPUs. We evaluate Spira on three NVIDIA GPUs, RTX 3090 (24GB), Tesla A100 (80GB) and Quadro RTX 5000 (16GB). Unless otherwise stated, we present detailed evaluation results on RTX 3090.

Neural Networks. We evaluate three point cloud networks: SparseResNet (21 layers) (**ResN**), MinkUNet (42 layers) (**UNet**) (Choy et al., 2019), and Centerpoint Large (20 layers) (**ResNL**) (Chen et al., 2023), which uses SpC layers with K=5 (instead of 3) in all stages of ResNet backbone.

Datasets. We evaluate three large-scale point cloud datasets: SemanticKITTI (**KITTI**) (Behley et al., 2019), which includes outdoor LiDAR scans for self-driving scenarios, **ScanNet** (Dai et al., 2017), which contains RGB-D scans of indoor environments, and **Waymo** (Sun et al., 2019), which provides large-scale outdoor scenes for automotive object detection. All experiments are using 16-bit float precision.

Comparison Points. We compare Spira with two state-of-the-art SpC engines: (i) Minuet and (ii) TorchSparse++. In Spira, we account for both sorting and packing the initial input coordinates. We do not include tuning time for any engine as tuning happens only once and is before inference.

6.2 End-to-End Inference Performance

Fig. 7 shows end-to-end inference performance of all engines across different point cloud networks, datasets and three GPUs. Spira uses 32-bit or 64-bit packed-native voxel indexing.

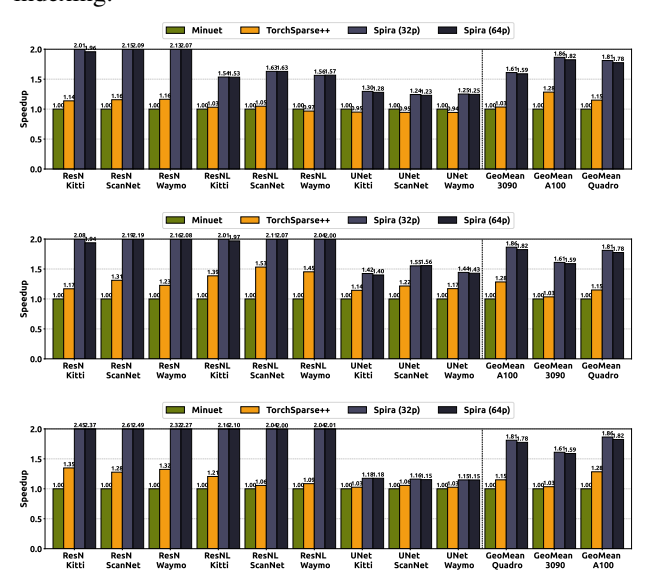


Figure 7. End-to-end inference performance on RTX 3090 (top), A100 (middle), and Quadro RTX 5000 (bottom).

We make three key observations. First, TorchSparse++ outperforms Minuet on ResN and ResNL networks, but achieves comparable performance on UNet. In ResN and ResNL networks, output-stationary dataflow performs better than weight-stationary in the majority of layers, while Minuet does not support output-stationary. In contrast, in UNet, weight-stationary outperforms output-stationary in most of the layers. Second, Spira with 64-bit coordinate packing versus 32-bit of has negligible performance impact, demonstrating that Spira can provide significant performance benefits even in highly demanding point cloud applications. The one-time coordinate packing and sorting costs on the initial input coordinates account only for 1.3% and 1.6% of total inference time on average for the 32-bit and 64-bit Spira, respectively. Across all datasets and networks, Spira selects different dataflows with minimal post-processing overheads. For example, in UNet, Spira uses output-stationary dataflow in $\sim 20\%$ of layers and weight-stationary for the rest, while in ResNL, it uses hybrid dual-dataflow with t=3 in 9 out of 17 submanifold layers with K=5. Third, Spira consistently achieves best performance among prior SpC engines, reaching up to $2.31 \times$ and $1.98 \times$ over Minuet and TorchSparse++, respectively, and $1.71\times$ on average across all networks, datasets and three GPUs. Spira significantly outperforms prior SpC engines across various GPU devices and architectures, including Ampere architecture (e.g., RTX 3090 and A100) and Turing architecture (e.g., Quadro). Overall, Spira achieves the best performance among state-of-the-art SpC engines, demonstrating robust efficiency across diverse point cloud networks, datasets, and GPU architectures.

6.3 Layerwise Performance

Since 64-bit and 32-bit packing perform comparably, our subsequent evaluations show Spira with 32-bit packing. We assess various layers configurations (input channels, output channels, kernel size). For fair comparison with prior work, we do measure the voxel indexing runtime in Spira for each evaluated layer. Fig. 8 shows layerwise performance of all engines for various layer configurations commonly found in state-of-the-art networks. For each layer, we report the geometric mean across all datasets. TorchSparse++ and Spira select the best-performing dataflow.

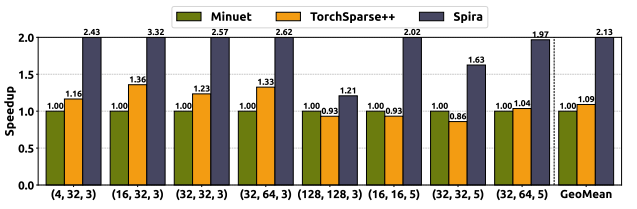


Figure 8. Layerwise speedup of all SpC engines averaged across all datasets, for various SpC layers of (C_{in}, C_{out}, K) .

We draw two findings. First, TorchSparse++ outperforms Minuet in layers with relatively small channels and kernel sizes (e.g., (16, 32, 3)) because, as we also explain in Fig. 9, output-stationary dataflow—which Minuet does not support—performs significantly better in such layers. However, in layers with larger channels and kernel sizes, TorchSparse++ achieves comparable performance to Minuet and even surpasses it in some cases. Second, Spira consistently outperforms Minuet and TorchSparse++ across all layers, delivering average speedup of $2.13\times$ and $1.95\times$ (up to $3.32\times$ and $2.44\times$), respectively. Spira uses t=3 in hybrid dual-dataflow for layers (16, 16, 5) and (32, 32, 5): although hybrid dual-dataflow still incurs post-processing costs, post-processing time is $5.41\times$ and $2.51\times$ lower on average than TorchSparse++ weight-stationary and Minuet, respectively.

Fig. 9 presents Spira layerwise performance using output-, weight-stationary or hybrid dual-dataflow varying the threshold t in submanifold layer configurations with s_p =1. For K=3 and K=5, t can get 3 and 6 values, respectively.

We draw two findings. First, output-stationary dataflow dominates in layers with smaller channels and kernel sizes. In such layers, weight-stationary incurs high postprocessing overhead relative to its feature computation time (actual convolution computation is relatively small). Conversely,

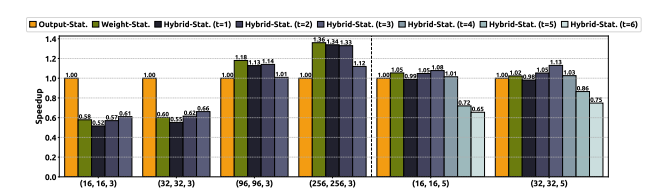


Figure 9. Layerwise Spira speedup with various dataflow schemes.

weight-stationary surpasses output-stationary in layers with larger channels and kernel sizes. For example, in layers with K=5, many weight offsets in kernel map are highly sparse, causing output-stationary to perform numerous unnecessary zero-valued multiplications. Second, hybrid dual-dataflow performs best in large layers with K=5, with speedups up to 1.13× and 1.11× over full output-stationary and full weightstationary, respectively, by combining the strengths of both dataflows. In layers with K=5 (125 weight offsets), thresholds $t \geq 5$ classify many weight offsets as dense (at least 93), causing high transposition overheads for the dense submatrix. Instead, threshold t=3 provides the best performance: it selects 25 weight offsets as dense (average density 32%) for output-stationary and 100 as sparse (average density 10%) for weight-stationary. This split effectively balances compute load across both dataflow executions, justifying the overheads of two separate GPU kernel launches.

6.4 Performance of Mapping in Voxel Indexing

Fig. 10 presents mapping performance (pre-processing and search phases of voxel indexing) for all SpC engines using real scenes from the evaluated datasets with varying input coordinate counts and layer kernel sizes. We add an additional baseline: lookup operations for kernel map construction are performed via simple binary search (**Simple BSearch**), which requires no pre-processing. Simple BSearch also includes 32-bit coordinate packing, as described in §5.3.

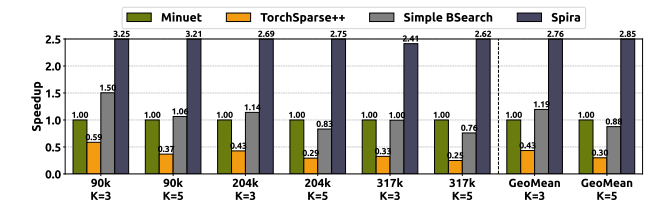


Figure 10. Mapping performance in voxel indexing for all engines across varying input coordinate counts and layer kernel sizes.

We make three key observations. First, Minuet clearly outperforms TorchSparse++ in all cases by $2.83 \times$ on average, as TorchSparse++ causes irregular memory accesses during lookups, while Minuet effectively exploits GPU on-chip caches. Second, Simple BSearch outperforms Minuet in smaller scenes (e.g., 90k voxels), but it scales poorly as the coordinate count and kernel size increase due to poor cache utilization. Third, Spira's z-delta search delivers outstanding performance over all comparison points across all scenes,

with speedup up to 2.85×, 9.49× and 3.45× over Minuet, TorchSparse++ and Simple BSearch, respectively. Minuet and TorchSparse++ exhibit notable pre-processing overhead of 8–36.5% and 18.3–55.5% of total mapping time, respectively. Instead, Spira *completely* eliminates pre-processing and significantly outperforms even packed-native Simple BSearch, which also has *no* pre-processing. Spira's z-delta search algorithm exploits the integer-valued property to perform intelligent localized searches: for many queries, it requires only a *single comparison* and a *single cache-friendly memory access*—while competing approaches perform multiple comparisons per query and may incur irregular memory accesses. This significantly reduces both computational cost and memory access latency, enabling robust performance even as coordinate counts and kernel sizes increase.

6.5 Performance Breakdown of Spira's Key Ideas

Fig. 11 shows performance benefits by incrementally adding Spira's optimizations: (1) 32-bit packed-native voxel indexing on Simple BSearch with output-stationary dataflow, (2) replacing Simple BSearch with Spira's z-delta search, and (3) replacing output-stationary with Spira's adaptive hybrid dual-dataflow. We evaluate a common layer of (C_{in}, C_{out}, K) =(32,32,5), which appears in 4 of 20 layers in ResNL, and include the voxel indexing runtime. We find that all Spira ideas significantly contribute to overall performance. The most substantial speedup comes from z-delta search algorithm (1.75× over TorchSparse++), demonstrating the effectiveness of its *one-shot* design (no preprocessing) and highly localized search scheme that is both compute and memory efficient. Spira's hybrid dual-dataflow yields additional improvements (1.98× over TorchSparse++).

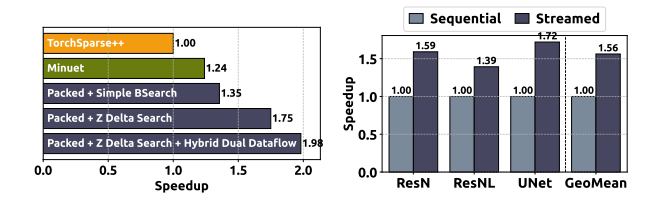


Figure 11. Performance break-Figure 12. Spira with sequential down of the key ideas of Spira. vs streamed voxel indexing.

Fig.12 shows the performance benefits of network-wide voxel indexing. We measure total voxel indexing time of all layers in three networks using either sequential execution or streamed (concurrent) execution across multiple GPU SMs (§5.5). Spira's network-wide streamed execution improves voxel indexing performance up to $1.72\times$ and end-to-end inference up to $1.12\times$ over sequential execution.

7 OTHER RELATED WORK

Point Cloud Accelerators. Prior works (Zhu et al., 2020; Feng et al., 2020; Han et al., 2024; Zhang & Zhang, 2021; Feng et al., 2022; Lin et al., 2021; 2024; Lyu et al., 2023)

propose application-specific accelerators for point cloud networks. However, only a few accelerators (Lin et al., 2021; 2024; Lyu et al., 2023) support the 3D SpC. These works have custom microarchitecture designs and rely on simulators for evaluation, which limits their immediate practical deployment. Instead, Spira is a software runtime engine that directly runs on commodity high-end and edge GPU, provides comprehensive evaluations on real systems, and enables immediate deployment in real SpC applications.

Deep Learning Compilers. Deep Learning (DL) compilers optimize dense tensor algebra (Feng et al., 2023; Chen et al., 2018; Ding et al., 2023; Xing et al., 2022) and sparse tensor algebra kernels (Gupta et al., 2025; Liu et al., 2025; Ahrens et al., 2025; Du et al., 2025; Won et al., 2023; Ye et al., 2023; Kjolstad et al., 2017). Although some sparse DL compilers could be used to optimize SpC, these compilers do not integrate the optimizations proposed in Spira. Spira's ideas can work synergistically with existing sparse DL compilers to significantly improve performance in SpC executions.

8 CONCLUSION

We introduce Spira, the first voxel-property-aware SpC engine for GPUs. Spira proposes the one-shot z-delta search algorithm that has low computational cost and high memory locality, integrates packed-native voxel indexing that significantly reduces data accesses, employs network-wide parallelization in voxel indexing kernels of all network's SpC layers to increase execution parallelism, and provides flexible hybrid dual-dataflow feature computation that adapts to layer characteristics. Spira significantly outperforms prior state-of-the-art SpC engines by $1.71\times$ on average and up to $2.31\times$ in end-to-end inference across various point cloud networks, real-world datasets, and GPUs. We hope Spira enables further research on sparse operators of ML models.

REFERENCES

- Ahrens, W., Collin, T. F., Patel, R., Deeds, K., Hong, C., and Amarasinghe, S. Finch: Sparse and Structured Tensor Programming with Control Flow. *Proc. ACM Program. Lang.*, 2025.
- Behley, J., Garbade, M., Milioto, A., Quenzel, J., Behnke, S., Stachniss, C., and Gall, J. A Dataset for Semantic Segmentation of Point Cloud Sequences. *CoRR*, abs/1904.01416, 2019. URL http://arxiv.org/abs/1904.01416.
- Chen, T., Moreau, T., Jiang, Z., Zheng, L., Yan, E., Shen, H., Cowan, M., Wang, L., Hu, Y., Ceze, L., Guestrin, C., and Krishnamurthy, A. TVM: An Automated Endto-End Optimizing Compiler for Deep Learning. In 13th USENIX Symposium on Operating Systems Design and Implementation (OSDI 18), 2018.

- Chen, Y., Liu, J., Zhang, X., Qi, X., and Jia, J. VoxelNeXt: Fully Sparse VoxelNet for 3D Object Detection and Tracking, 2023. URL https://arxiv.org/abs/2303.11301.
- Choy, C., Gwak, J., and Savarese, S. 4D Spatio-Temporal ConvNets: Minkowski Convolutional Neural Networks. In 2019 IEEE/CVF Conference on Computer Vision and Pattern Recognition (CVPR), 2019.
- Dai, A., Chang, A. X., Savva, M., Halber, M., Funkhouser, T., and Nießner, M. ScanNet: Richly-annotated 3D Reconstructions of Indoor Scenes, 2017. URL https://arxiv.org/abs/1702.04405.
- Ding, Y., Yu, C. H., Zheng, B., Liu, Y., Wang, Y., and Pekhimenko, G. Hidet: Task-Mapping Programming Paradigm for Deep Learning Tensor Programs. In *Proceedings of the 28th ACM International Conference on Architectural Support for Programming Languages and Operating Systems*, Volume 2, 2023.
- Du, Z., Liu, Y., Sun, N., Cui, H., Feng, X., and Li, J. SRSparse: Generating Codes for High-Performance Sparse Matrix-Vector Semiring Computations. ACM Trans. Archit. Code Optim., 2025.
- Feng, S., Hou, B., Jin, H., Lin, W., Shao, J., Lai, R., Ye, Z., Zheng, L., Yu, C. H., Yu, Y., et al. TensorIR: An Abstraction for Automatic Tensorized Program Optimization. In Proceedings of the 28th ACM International Conference on Architectural Support for Programming Languages and Operating Systems, Volume 2, pp. 804–817, 2023.
- Feng, Y., Tian, B., Xu, T., Whatmough, P., and Zhu, Y. Mesorasi: Architecture Support for Point Cloud Analytics via Delayed-Aggregation. In 2020 53rd Annual IEEE/ACM International Symposium on Microarchitecture (MICRO), 2020.
- Feng, Y., Hammonds, G., Gan, Y., and Zhu, Y. Crescent: Taming Memory Irregularities for Accelerating Deep Point Cloud Analytics. In *Proceedings of the 49th Annual International Symposium on Computer Architecture*, 2022.
- GitHub, T. Torchsparse++ github. https://github.com/mit-han-lab/torchsparse, 2025.
- Gupta, A., Yuan, Y., Jain, D., Ge, Y., Aponte, D., Zhou, Y., and Mendis, C. SPLAT: A Framework for Optimised GPU Code-Generation for SParse regular ATtention. *Proc. ACM Program. Lang.*, 2025.
- Han, M., Wang, L., Xiao, L., Zhang, H., Cai, T., Xu, J., Wu, Y., Zhang, C., and Xu, X. BitNN: A Bit-Serial Accelerator for K-Nearest Neighbor Search in Point Clouds. In 2024 ACM/IEEE 51st Annual International Symposium on Computer Architecture (ISCA), 2024.

- Hong, K., Yu, Z., Dai, G., Yang, X., Lian, Y., Xu, N., and Wang, Y. Exploiting Hardware Utilization and Adaptive Dataflow for Efficient Sparse Convolution in 3D Point Clouds. *Proceedings of Machine Learning and Systems*, 2023.
- Kim, P., Chen, J., and Cho, Y. K. SLAM-driven Robotic Mapping and Registration of 3D Point Clouds. *Automation in Construction*, 89:38–48, 2018.
- Kjolstad, F., Kamil, S., Chou, S., Lugato, D., and Amarasinghe, S. The Tensor Algebra Compiler. *Proc. ACM Program. Lang.*, (OOPSLA), 2017.
- Lin, X., Huang, S., and Jiang, H. Voxel-CIM: An Efficient Compute-in-Memory Accelerator for Voxel-based Point Cloud Neural Networks. In *Proceedings of the 43rd IEEE/ACM International Conference on Computer-Aided Design*, pp. 1–9, 2024.
- Lin, Y., Zhang, Z., Tang, H., Wang, H., and Han, S. PointAcc: Efficient Point Cloud Accelerator. In MICRO-54: 54th Annual IEEE/ACM International Symposium on Microarchitecture, 2021.
- Liu, F., Huang, S., Yang, N., Wang, Z., Li, H., and Jiang, L. CROSS: Compiler-Driven Optimization of Sparse DNNs Using Sparse/Dense Computation Kernels. In 2025 IEEE International Symposium on High Performance Computer Architecture (HPCA), 2025.
- Lyu, D., Li, Z., Chen, Y., Zhang, J., Xu, N., and He, G. SpOctA: A 3D Sparse Convolution Accelerator with Octree-Encoding-Based Map Search and Inherent Sparsity-Aware Processing. *arXiv* preprint *arXiv*:2308.09249, 2023.
- Spconv2. Spconv: Spatially sparse convolution library. https://github.com/traveller59/spconv, 2022.
- Sun, P., Kretzschmar, H., Dotiwalla, X., Chouard, A., Patnaik, V., Tsui, P., Guo, J., Zhou, Y., Chai, Y., Caine, B., Vasudevan, V., Han, W., Ngiam, J., Zhao, H., Timofeev, A., Ettinger, S., Krivokon, M., Gao, A., Joshi, A., Zhang, Y., Shlens, J., Chen, Z., and Anguelov, D. Scalability in Perception for Autonomous Driving: Waymo Open Dataset. *CoRR*, abs/1912.04838, 2019. URL http://arxiv.org/abs/1912.04838.
- Tang, H., Liu, Z., Li, X., Lin, Y., and Han, S. Torchsparse: Efficient Point Cloud Inference Engine. *Proceedings of Machine Learning and Systems*, 4:302–315, 2022.
- Tang, H., Yang, S., Liu, Z., Hong, K., Yu, Z., Li, X., Dai, G., Wang, Y., and Han, S. TorchSparse++: Efficient Training and Inference Framework for Sparse Convolution on GPUs. In *Proceedings of the 56th Annual IEEE/ACM International Symposium on Microarchitecture*, 2023.

- Wirth, F., Quehl, J., Ota, J., and Stiller, C. Pointatme: Efficient 3D Point Cloud Labeling in Virtual Reality. In 2019 IEEE Intelligent Vehicles Symposium (IV), pp. 1693–1698. IEEE, 2019.
- Won, J., Hong, C., Mendis, C., Emer, J., and Amarasinghe, S. Unified Convolution Framework: A Compiler-Based Approach to Support Sparse Convolutions. *Proceedings* of Machine Learning and Systems, 5:666–679, 2023.
- Wu, W., Qi, Z., and Fuxin, L. PointConv: Deep Convolutional Networks on 3D Point Clouds. In *Proceedings* of the IEEE/CVF Conference on computer vision and pattern recognition, pp. 9621–9630, 2019.
- Xing, J., Wang, L., Zhang, S., Chen, J., Chen, A., and Zhu, Y. Bolt: Bridging the Gap Between Auto-Tuners and Hardware-Native Performance. *Proceedings of Machine Learning and Systems*, 2022.
- Yang, J., Giannoula, C., Wu, J., Elhoushi, M., Gleeson, J., and Pekhimenko, G. Minuet: Accelerating 3D Sparse Convolutions on GPUs. In *Proceedings of the Nineteenth European Conference on Computer Systems*, 2024.
- Ye, Z., Lai, R., Shao, J., Chen, T., and Ceze, L. SparseTIR: Composable Abstractions for Sparse Compilation in Deep Learning. In *Proceedings of the 28th ACM International Conference on Architectural Support for Programming Languages and Operating Systems, Volume 3*, 2023.
- Yin, T., Zhou, X., and Krahenbuhl, P. Center-Based 3D Object Detection and Tracking. In *Proceedings of the IEEE/CVF conference on computer vision and pattern recognition*, pp. 11784–11793, 2021.
- Zermas, D., Izzat, I., and Papanikolopoulos, N. Fast Segmentation of 3D Point Clouds: A Paradigm on LiDAR Data for Autonomous Vehicle Applications. In 2017 IEEE International Conference on Robotics and Automation (ICRA), pp. 5067–5073. IEEE, 2017.
- Zhang, J.-F. and Zhang, Z. Point-X: A Spatial-Locality-Aware Architecture for Energy-Efficient Graph-Based Point-Cloud Deep Learning. In *MICRO-54: 54th Annual IEEE/ACM International Symposium on Microarchitecture*, 2021.
- Zheng, Z., Bewley, T. R., and Kuester, F. Point Cloud-Based Target-Oriented 3D Path Planning for UAVs. In 2020 International conference on unmanned aircraft systems (ICUAS), pp. 790–798. IEEE, 2020.
- Zhu, C., Huang, K., Yang, S., Zhu, Z., Zhang, H., and Shen, H. An Efficient Hardware Accelerator for Structured Sparse Convolutional Neural Networks on FPGAs. *IEEE Transactions on Very Large Scale Integration (VLSI) Systems*, 2020.

Zhu, X., Zhou, H., Wang, T., Hong, F., Ma, Y., Li, W., Li, H., and Lin, D. Cylindrical and Asymmetrical 3D Convolution Networks for Lidar Segmentation. In *Proceedings of the IEEE/CVF conference on computer vision and pattern recognition*, pp. 9939–9948, 2021.